AIAA JOURNAL
Vol. 46, No. 7, July 2008

Aerodynamic Optimization of Essentially Three-Dimensional Shapes for Wing–Body Fairing

Sergey Peigin*
Israel Aerospace Industries, Ltd., 70100 Ben-Gurion Airport, Israel
and
Boris Epstein†
Academic College of Tel-Aviv-Yaffo, 64044 Tel-Aviv, Israel

DOI: 10.2514/1.35465

A new approach for the optimization of essentially three-dimensional aerodynamic shapes for minimum drag is proposed. The method allows the handling of the nonlinear surfaces that are typical of complex aircraft junctions such as a wing–body fairing. The optimization framework OPTIMAS, previously proposed and developed by the authors for the solution of the drag-minimization problem for two-dimensional airfoils, three-dimensional isolated wings, and three-dimensional wings in the presence of a body in succession, is extended in this paper to a significantly higher level of geometrical complexity of optimized aerodynamic configurations. The method is driven by accurate full Navier–Stokes evaluations of the objective function, and the optimization engine is based on genetic algorithms. The important features of the method are the ability to accurately handle multiple geometrical/aerodynamic constraints and a high level of computational efficiency, achieved through massive multilevel parallelization and a reduced-order-model approach. The method was applied to the optimization of a wing–body fairing for a generic business jet configuration at realistic transonic cruise flight conditions. The results demonstrate that the proposed approach achieves significant drag reduction in on- and offdesign conditions and can be used in an engineering environment.

I. Introduction

THE use of computational fluid dynamics (CFD)-driven aerodynamic shape optimizers may significantly reduce the overall cost of industrial aerodynamic design. The first aerodynamic optimization method was proposed by Lighthill [1] more than 60 years ago (it consisted of the use of conformal mapping for the design of two-dimensional airfoils). In succeeding years, the development of aerodynamic optimization methods was correlated with the concurrent progress in three major directions.

Within the first line of development, following the progress in computational fluid dynamics, increasingly advanced gas-dynamic models for the evaluation of objective function were employed [2]: from linear and full potential equations [3] through Euler equations (sometimes coupled with boundary-layer equations) [4–7] to full Navier–Stokes equations [8,9].

The second direction is associated with the increase in geometrical complexity of optimized configurations: from 2-D airfoils [1,4] through isolated 3-D wings [9,10] and blended wing–body shapes [11] to three-dimensional wings incorporated in full aircraft configuration [12–14].

The third major direction is related to the progress in optimization techniques in terms of search efficiency, globality, and constraint handling. In this connection, the idea to compute the gradient direction through the adjoint equation approach [6,15] was a leap forward in improving the computational efficiency of optimization. Though the majority of publications on the subject stem from this approach, the necessity to improve the globality of optimum search stimulated the use of evolutionary methods [16,17].

The authors have a good reason to think that to be really incorporated in the engineering practice, an industrial optimization tool should be based on full Navier–Stokes computations, global optimization technique, and efficient and accurate handling of multiple geometrical/aerodynamic constraints and should be applicable to a sufficiently wide range of optimized aerodynamic configurations and design conditions.

This is why, prompted by industrial requests in recent years, the authors have proposed and developed the new accurate, robust, and computationally efficient design tool OPTIMAS (optimization of aerodynamic shapes) for multipoint multiconstrained optimization of aerodynamic shapes, applicable to 2-D airfoils, 3-D isolated wings, and 3-D wings in the presence of aircraft fuselage [18–21].

Nevertheless, notwithstanding the advancement in expanding the range of geometrical applicability, the practical impact of the developed approach was limited by the optimization of linear/quasi-linear shapes, such as ruled surfaces. At the same time, in practical aerodynamic design of civil aircraft, the optimization of essentially nonlinear 3-D surfaces (typical of complex aircraft junctions) is of crucial importance.

To the best of the authors' knowledge, the problem of optimizing such shapes remains open until the present time. The reason apparently lies in the fact that the solution of this problem requires very accurate numerical simulations of complex 3-D viscous/inviscid flow interaction, along with global geometrical representation of the optimized nonlinear surfaces. Though the optimization methods based on local representation of optimized surfaces do not place specific requirements upon geometrical complexity of the surfaces (see [7,8]), nevertheless, no publications dealing with CFD-driven optimization of the wing–body fairing are available to the authors.

With the purpose of resolving the preceding problem, in this paper, the approach for optimizing essentially 3-D aerodynamic shapes for minimum drag is proposed. The method allows the efficient handling of essentially 3-D nonlinear surfaces typical of complex aircraft junctions such as wing–body fairing and thus extends the capabilities of the optimization framework OPTIMAS to a significantly higher level of geometrical complexity of optimized aerodynamic configurations. The method is based on the high-fidelity complete

Received 7 November 2007; revision received 5 February 2008; accepted for publication 10 March 2008.

*Professor, Engineering Division. Senior Member AIAA.
†Professor, Computer Sciences Department, 4 Antokolsky Street. Member AIAA.

aerodynamic model (Navier–Stokes computations), expands the globality of optimum search [by employing mixed deterministic/probabilistic genetic algorithms (GAs)], and simultaneously handles a large number of constraints.

In industry, the success of a method should be assessed through practical optimization of realistic aerodynamic configurations. In this paper, we illustrate the capabilities of the method by applying it to the optimization of the wing–body fairing for a generic business jet configuration at realistic transonic cruise flight conditions. The results demonstrate that the proposed approach achieves significant drag reduction in on- and offdesign conditions and can be used in the engineering environment. It was shown that the optimization of the wing–body fairing can considerably improve the aerodynamic performance of the aircraft in comparison with the previous design, in which only wing surface of the generic business jet was subject to optimization.

II. Statement of the Problem

The design goal is to optimize a given aircraft configuration for minimum drag at specified design conditions subject to constraints placed upon the solution. This objective is accomplished through the solution of the constrained optimization problem, with the total drag coefficient C_D as an objective function:

$$f^{\text{objective}} = C_D$$

The optimal solution is also required to satisfy the geometrical constraints imposed in terms of optimized surface properties and aerodynamic constraints such as prescribed lift coefficient C_L^*, and maximum-allowed pitching moment C_M^*:

$$C_L = C_L^*, \qquad C_M \geq C_M^* \tag{1}$$

The gas-dynamic model for estimating C_D, C_L, and C_M values are the full Navier–Stokes equations. The effects of turbulence are modeled through an eddy-viscosity hypothesis with the Baldwin and Lomax [22] turbulence model. The numerical solution of these equations was provided by the multiblock code NES [23], which employs structured point-to-point matched grids. The code is based on the essentially nonoscillatory concept with a flux interpolation technique [24], which allows accurate estimation of sensitive aerodynamic characteristics such as lift, pressure drag, friction drag, and pitching moment. As a result, the code ensures high accuracy of the Navier–Stokes computations and high robustness for a wide range of flows and geometrical configurations, even on relatively coarse meshes, and thus allows a dramatic reduction in the amount of CFD computations.

III. Optimization Algorithm

A. Optimum Search

The optimization technique uses a genetic algorithm as its search engine. GAs became highly popular as optimization methods in the last two decades. Relevant survey articles that include industrial applications could be found in [25]. The basic idea behind genetic algorithms is to mathematically imitate the evolution process of nature. They are semistochastic optimization methods that are conveniently presented using the metaphor of natural evolution: a randomly initialized population of individuals (set of points of the search space at hand) evolves following a crude parody of the Darwinian principle of the survival of the fittest. The main point is that the probability of survival of new individuals depends on their fitness: the best are kept with a high probability, and the worst are rapidly discarded.

As a basic algorithm, a variant of the floating-point GA is employed [26]. We used the tournament selection, which enables us to increase the diversity of the parents, single-point crossover operator, nonuniform mutation [27], and elitism principle.

The constraint handling can be basically outlined as follows (for more detail, see [28]):

1) Instead of the traditional approach in which only feasible points may be included in a path, it is proposed to employ search paths through both feasible and infeasible points

2) With this end in view, the search space is extended by evaluating (in terms of fitness) the points that do not satisfy the constraints imposed by the optimization problem. A needed extension of an objective function may be implemented due to a basic property of GAs: contrary to classical optimization methods, GAs are not confined to only smooth extensions.

The major weakness of GAs lies in their poor computational efficiency, which prevents the practical use when the evaluation of the cost function is expensive, as happens in the framework of the full Navier–Stokes model. One of the popular ways of overcoming this difficulty is to use a reduced-order-model approach in the broadest sense of the word. Among these, we may mention the use of simpler gas-dynamic models (see, for example, [29]), representation of the solution of gas-dynamic problem in terms of its eigenmodes [30], or representation of the aerodynamic system using the Volterra theory of nonlinear systems [31].

To improve the computational efficiency of the GA search algorithm while keeping the population to the representative level, we use a reduced-order-model approach in the form of a local-approximation method, in which the solution functionals are approximated by a local database. The database is obtained by solving the full Navier–Stokes equations in a discrete neighborhood of a basic point (basic geometry) positioned in the search space. Specifically, a mixed linear-quadratic approximation is employed. One-dimensionally, the one-sided linear approximation is used in the case of monotonic behavior of the approximated function, and the quadratic approximation is used otherwise.

To ensure the accuracy and robustness of the method, a multidomain prediction–verification principle is employed. That is, at the prediction stage, the genetic optimum search is concurrently performed on a number of search domains. As a result, each domain produces an optimal point, and the whole set of these points is verified (through full Navier–Stokes computations) on the verification stage of the method, and thus the final optimal point is determined.

In addition, to ensure the global character of the search, it is necessary to overcome the local nature of the preceding approximation. For this purpose, it is proposed to perform iterations in such a way that in each iteration, the result of optimization serves as the initial point for the next iteration step (further referred to as the optimization step).

To additionally improve the computational efficiency of the tool, we employ an embedded multilevel parallelization strategy [32] of the whole computational framework, which efficiently makes use of computational power supplied by massively parallel processors.

The general sketch of the optimization algorithm can be presented by the pseudocode in Algorithm 1.

B. Search-Space Parameterization

An optimization process can be described as a path in the search space, the points of which represent different geometries. Thus, the choice of an appropriate search space is of crucial importance. In practice, the initial geometry of the configuration comes in the form of a CAD representation or as an already 3-D numerical grid (needed for CFD estimation of the objective function). Note that in the former case, the CAD files should be converted into a CFD grid. In both cases, an aerodynamic surface is represented by a set of local patches, and each patch is a set of discrete points. The total number of surface points may amount to 100,000.

The search space should include a sufficiently wide spectrum of geometrical shapes. The preceding local shape satisfies this requirement, but results in very high dimensions of the search space. On the other hand, because the complexity of the optimal search grows exponentially with the search-space dimensions, the total number of parameters should not be too high (to ensure a successful and efficient search). Hence, a global representation of aerodynamic surfaces is needed. The main requirements for such a representation

Algorithm 1 Pseudocode for the optimization algorithm

opt_step=0	
Determine_Initial_Basic_Point	Starting basic point: initial geometry
while not converged do	
Calc_Local_Data_Base	CFD computations in a discrete neighborhood of the basic point
Search_Optim_Candidates	Hybrid GA and reduced-order-model/local-approximation-method search of optimal points for various search domains
Verification_Optim_Cand	CFD computations for optimal points
Choose_New_Basic_point	Choose a new basic point: the best one among all the points in the global CFD database
opt_step=opt step+1	
enddo	

are the following. It should be based on a limited number of parameters and should ensure a sufficient shape representativeness; additionally, points that are close to each other in the search space should yield close CFD grids.

In the preceding publications on the subject of aerodynamic shape optimization, the parametrization proposed and employed by the authors (see [19–21,33]) was related to linear [or quasi-linear (ruled)] surfaces. Within the previously developed framework, the wing (or quasi wing, as in [20]) surface was generated by a linear spanwise interpolation of 2-D sectional cuts, and the shape of each cut was determined by one-parameter Bezier splines. Additional parameters of optimization were twists and dihedrals of the cuts, and the wing planform remained fixed. This approach, though quite successful for the parameterization of the winglike surface, could not be applied to a description of real 3-D surfaces such as a wing–body fairing. That is why, in the present work, the surface of fairing was parameterized by means of two-parameter Bezier surfaces.

The whole surface may be optimized either by a simultaneous optimization of the wing and wing–body fairing or, alternatively, by a successive optimization of the exposed wing (the wing surface outboard of the fairing) and the fairing itself. The second mode, which may require a small number of iterations, makes it possible to estimate the contribution of each optimized surface in the buildup of the optimization gain. In the present work, the second mode was adopted due to its higher relevance in the engineering context, in which the already existing wing may not be subject to modification. The implementation of the first combined mode is planned in the future.

In the following, it is assumed that the geometry of the aircraft configuration is described in the absolute Cartesian coordinate system (x, y, z), in which the axes x, y, and z are directed along the streamwise, normal to wing surface, and span directions, respectively. In the developed approach, the whole surface of a wing–body configuration is divided into three parts. The first part contains the points of the aircraft fuselage inboard of the fairing. This part of the configuration is not subject to modification.

The second part contains the points of the exposed-wing outboard of the fairing. This part of the configuration is represented by a linear interpolation of 2-D cuts (wing sections). For each wing section, the nondimensional shape of the airfoil (scaled by the corresponding chord) is defined in a local Cartesian coordinate system $(\bar{x}, \bar{y})$ in the following way. The coordinates of the leading edge and trailing edge of the profile were, respectively, (0, 0) and (1, 0). For approximation of the upper and lower airfoil surface, Bezier curve (one-dimensional Bezier spline) representation was used. A Bezier curve of order N is defined by the Bernstein polynomials $B_{N,i}$ (C_N^i for binomial coefficients):

$$\mathbf{G}^k(t) = \sum_{i=0}^{N} B_{N,i}\mathbf{P}_i^k, \qquad B_{N,i} = C_N^i t^i (1-t)^{N-i}, \qquad C_N^i = \frac{N!}{i!(N-i)!} \tag{2}$$

where t denotes the curve parameter taking values in [0, 1], $\mathbf{P}_i^k$ are the control points (superscript $k = u,l$ corresponds to the upper and lower surfaces of the profile). As shown in Eq. (2), the Bezier curve is completely determined by the Cartesian coordinates of the control points. Additional parameters of optimization are twist angles $\{\alpha_i^{\text{tw}}\}$ and dihedral values $\{\gamma_i^{\text{dh}}\}$. In total, in the framework of the exposed-wing optimization, 38 design variables were used.

Finally, the third (highly nonlinear) part of the configuration is the fairing. This essentially 3-D part is described through combination of Bezier surfaces representation (two-parameter families of Bezier splines) and local twist distribution (one-parameter Bezier spline). To do this, we introduce a local Cartesian coordinate system $(\bar{x}, \bar{y}, \bar{z})$ in the following way:

$$\bar{x} = \frac{x^{\text{new}} - x_{\text{LE}}^{\text{new}}}{C(z)}, \qquad \bar{y} = \frac{y^{\text{new}} - y_{\text{TE}}^{\text{new}}}{C(z)}, \qquad \bar{z} = \frac{z - z_{\text{IB}}}{z_{\text{OB}} - z_{\text{IB}}},$$
$$x^{\text{new}} = x_{\text{TE}} + (x - x_{\text{TE}})\cos\alpha(z) - (y - y_{\text{TE}})\sin\alpha(z),$$
$$y^{\text{new}} = y_{\text{TE}} + (y - y_{\text{TE}})\cos\alpha(z) + (x - x_{\text{TE}})\sin\alpha(z),$$
$$\sin\alpha = \frac{y_{\text{LE}} - y_{\text{TE}}}{C(z)}$$

where subscripts LE and TE correspond to points located on the leading edge and trailing edge of the fairing, subscripts IB and OB correspond to points that belong to the inboard and outboard fairing sections, and $C(z)$ and $\alpha(z)$ are the chord value and twist angle of the fairing section at the current spanwise coordinate z.

Note that in the preceding local Cartesian coordinate system, we get

$$\bar{x}(x_{\text{LE}}, y_{\text{LE}}, z_{\text{LE}}) = 0, \qquad \bar{x}(x_{\text{TE}}, y_{\text{TE}}, z_{\text{TE}}) = 1,$$
$$\bar{y}(x_{\text{LE}}, y_{\text{LE}}, z_{\text{LE}}) = 0, \qquad \bar{y}(x_{\text{TE}}, y_{\text{TE}}, z_{\text{TE}}) = 0,$$
$$\bar{z}(x_{\text{IB}}, y_{\text{IB}}, z_{\text{IB}}) = 0, \qquad \bar{z}(x_{\text{OB}}, y_{\text{OB}}, z_{\text{OB}}) = 1$$

In this coordinate system, with the inboard and outboard sections of the fairing fixed, the nondimensional shape of the fairing and local twist distribution α are defined in the following way:

$$\mathbf{G}^k(t,s) = \sum_{i=0}^{N}\sum_{j=0}^{M} \mathbf{P}_{ij}^k B_{N,i}(t) B_{M,j}(s), \qquad \alpha(s) = \sum_{j=0}^{M} \alpha_j B_{M,j}(s),$$
$$B_{N,i}(t) = C_N^i t^i (1-t)^{N-i}, \qquad B_{M,j}(s) = C_M^j s^j (1-s)^{M-j}, \tag{3}$$
$$C_N^i = \frac{N!}{i!(N-i)!}, \qquad C_M^j = \frac{M!}{j!(M-j)!}$$

where t and s denote the surface parameters taking values in [0, 1], $\mathbf{P}_{ij}^k$ and α_j are the control points (superscript $k = u,l$ corresponds to the upper and lower surfaces of the wing–body fairing). Note that Bezier surfaces of Eq. (3) represent the geometry itself (contrary to the possibility of representing the deformation value from the original configuration).

For the optimization problem considered, the coordinate $\bar{y}$ of the control points $\mathbf{P}_{0j}^k$ and $\mathbf{P}_{Nj}^k$ ($k = u,l$ and $j = 0, \ldots, M$) is set to zero just by fixing the position of the leading and trailing edges. We also fix all the coordinates $\bar{x}_{ij}^k$ and $\bar{z}_{ij}^k$ of the control points $\mathbf{P}_{ij}^k$. We set $\bar{x}_{1j}^k = 0$ to ensure that the upper and lower surfaces of the fairing are tangent to the $\bar{y}$ axes at the leading edge. Additionally, assuming the continuity of the fairing curvature at the leading edge, we obtain the relations $\bar{y}_{1j}^u = -\bar{y}_{1j}^l$. Finally, we do not change any of the coordinates of the control points $\mathbf{P}_{i0}^k$, $\mathbf{P}_{iM}^k$, α_0, and α_M, to fix the location of the inboard and outboard wing-fairing sections. Thus, the shape of a wing–body fairing is completely determined by a total of $(2N-2)(M-1)$ parameters

$$S = (a_1, \ldots, a_{(2N-2)\cdot(M-1)})$$

which contains $\bar{y}^u_{ij}$ $(i = 1, \ldots, N-1,\ \ j = 1, \ldots, M-1)$, $\bar{y}^l_{ij}$ $(i = 2, \ldots, N-1,\ j = 1, \ldots, M-1)$, and α_j $(j = 1, \ldots, M-1)$. Thus, the dimensions N_D of the search space are equal to

$$N_D = (2N-2)\cdot(M-1)$$

In practice, we used $N = 10$ and $M = 4$, making N_D equal to 54.

Finally, a search string S contains N_D floating-point variables a_j $(j = 1, \ldots, N_D)$ and the string components are varied within the search domain D. The domain D is determined by a set of values $\min_j$ and $\max_j$, which are the lower and upper bounds of the variable a_j. Note that the detailed analysis demonstrates that the preceding described surface parameterization exhibits a sufficient shape representation. For example, such parameterization allows approximating the original fairing with an accuracy of about 0.3 mm (required in engineering practice). Additionally, the information about the variety of shapes treated in the framework of the optimization can be found in Fig. 1, in which the original fairing cut at $s = 0.4$ is compared with the corresponding cuts for the upper and lower bounds of design variables.

C. Treatment of CFD Meshes

The construction of local databases necessitates multiple full Navier–Stokes computations for different geometries. This requires the construction of multiple new CFD grids. To maintain the continuity of the optimization stream, we use a fast automatic transformation of the initial grid that corresponds to the starting basic geometry. This procedure is based on the topological similarity of all the considered geometrical configurations to the initial geometry.

Specifically, the implementation of the automatic fast grid transformation was as follows. First, the aircraft surface was divided into four parts. The first part comprises the fuselage surface points up to the inboard fairing section, and the second part (fairing itself) includes the surface points lying between the inboard and outboard wing-fairing sections. The last two parts are the exposed-wing region (between the outboard fairing section up to $z = z_{\text{tip}}$) and the tip region ($z > z_{\text{tip}}$).

The transformation of the initial basic grid includes two stages and is applied to all the grid blocks that contain the grid points located at the surface. Assume that the grid possesses an i, j, k structure, with the coordinate plane $j = 0$ representing the grid points lying on the configuration surface. Denote $\Delta\mathbf{r}_{i,0,k}$ as the change in the geometry of the surface at a grid point with indices $i, 0, k$. For the second and the third parts, $\Delta\mathbf{r}_{i,0,k}$ represent the differences between the current and the basic geometries. For the tip region (the fourth part), $\Delta\mathbf{r}_{i,0,k}$ are determined in a way that ensures a smooth blending of this part with the exposed-wing region. For the first part of the surface partition (the fuselage region), the corresponding $\Delta\mathbf{r}_{i,0,k}$ values are set to zero.

During the first stage, the coordinates $\mathbf{r}^{\text{new}}_{i,0,k}$ of the new grid for the all points located on the aircraft surface are calculated:

$$\mathbf{r}^{\text{new}}_{i,0,k} = \mathbf{r}^{\text{initial}}_{i,0,k} + \Delta\mathbf{r}_{i,0,k}$$

During the second stage, the coordinates $\mathbf{r}^{\text{new}}_{i,j,k}$ $(j > 1)$ of the new grid for the remaining points located outside the aircraft surface are computed by propagation of the scaled shift $\Delta\mathbf{r}_{i,0,k}$ along the grid lines $i = \text{const}$ and $k = \text{const}$:

$$\mathbf{r}^{\text{new}}_{i,j,k} = \mathbf{r}^{\text{initial}}_{i,j,k} + 0.5\left[1 + \cos\left(\pi\frac{j-1}{j_{\max}-1}\right)\right]\Delta\mathbf{r}_{i,0,k}$$

Finally, the deformed-mesh quality was examined with respect to the orthogonality and the Jacobian function of the grid cells. It was found that for all the considered optimizations, the quality of the deformed meshes were kept on the level of the original grid.

IV. Analysis of the Results

The method was applied to the problem of a single-point multiconstrained optimization of the wing–body–fairing surface for a generic business jet aircraft at transonic flight conditions. The configuration includes a realistic fuselage, a wing–body fillet, and a cranked glovelike high-aspect-ratio wing. The results of a previous multipoint constrained optimization of the exposed wing of this generic jet were presented by the authors in [21]. In terms of the present work, these optimizations can be considered as optimizations of the exposed-wing surface with the frozen shape of the wing–body fairing.

The CFD driver of the optimization process was the Israel Aerospace Industries in-house solver NES, which ensures high accuracy of the Navier–Stokes computations on relatively coarse grids, as well as high robustness, for a wide range of flows and geometrical configurations. For transonic wing–body configurations, NES provides accurate asymptotically converged estimates of aerodynamic coefficients with C-O topology grids containing on the fine level about 325 points around the configuration, 57 points normal to the surface, and 49 points in the spanwise direction. Specifically, for the considered generic business jet wing–body shape, the code NES was verified through systematic comparison with experimental data. An example of the comparison is given in Fig. 2, in which the drag polars at $M = 0.80$ are presented.

In the following, we present the results of a one-point drag minimization for a generic business jet aircraft. Note that at the design conditions, the original wing–body fairing did not produce separation at the side of the body. The geometrical constraints (applied to each section of the exposed wing) were placed upon a relative maximum-thickness local relative leading-edge radius and trailing-edge angle, as well as upon a relative local thickness at two fixed x/c locations (beam constraints). An additional (aerodynamic) constraint was imposed on the value of the pitching moment. In all the considered test cases, the values of all the preceding geometrical constraints were kept to the level of the original geometry. The design conditions and constraints are summarized in Table 1. The corresponding optimal shapes are designated as case GBJFR 1 to case GBJFR 4.

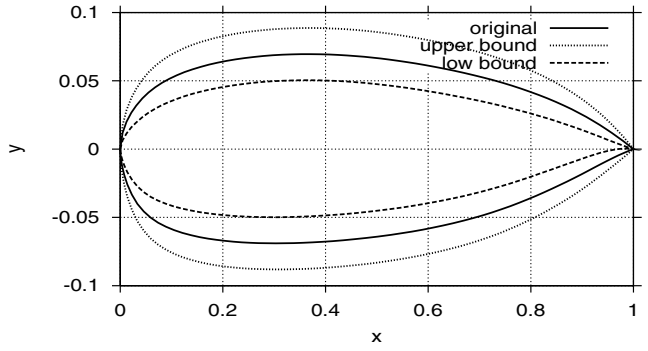

Fig. 1 Shape of sectional cuts in the fairing region at $s = 0.4$ for original vs upper and lower bounds of design variables.

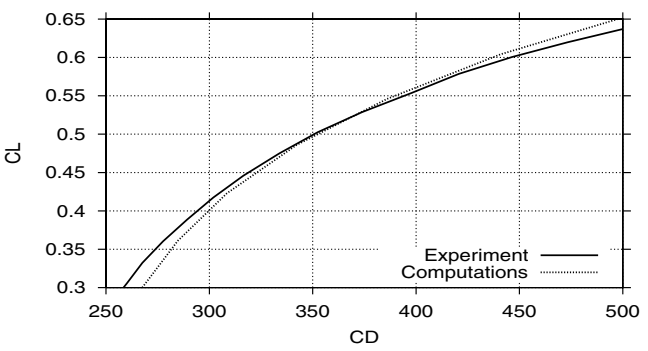

Fig. 2 Generic business jet wing–body drag polars at $M = 0.80$ for numerical computations vs experimental data.

Table 1 Generic business jet aircraft optimization conditions and constraints

Case no.	C_L^*	M	C_M^*	Beam	Fairing mode	Wing mode	Initial geometry	C_D
GBJFR 1	0.40	0.80	$-\infty$	no	yes	no	GBJ 2	264.6 counts
GBJFR 2	0.40	0.80	$-\infty$	no	no	yes	GBJFR 1	258.7 counts
GBJFR 3	0.40	0.80	−0.136	yes	yes	no	GBJ 5	269.2 counts
GBJFR 4	0.40	0.80	−0.136	yes	no	yes	GBJFR 3	259.1 counts

For the subsequent discussion, we will consider the following three initial geometries of the generic business jet: the original geometry and two geometries with an already optimized exposed wing, which were presented in [21] and labeled as case GBJ 2 (no constraint on C_M) and case GBJ 5 (with constraint on the pitching moment).

The test case GBJFR 1 deals with fairing optimization (with frozen exposed wing) without constraint on the pitching moment and without beam constraints. The initial geometry for this optimization came from case GBJ 2. The next test case (case GBJFR 2) deals with wing optimization with the frozen wing–body fairing resulting from the case GBJFR 1 optimization.

The last two test cases (case GBJFR 3 and case GBJFR 4) correspond to optimization with constraint on C_M and with beam constraints, which were kept to the original level. For case GBJFR 3 (fairing optimization with frozen optimal wing), the initial geometry was case GBJ 5, and for case GBJFR 4 (exposed-wing optimization with frozen optimal fairing), the initial geometry was the optimal shape of case GBJFR 3.

As already mentioned, the optimization method is iterative. The angle of attack was adjusted in CFD iterations to satisfy the target C_L value. As a whole, the algorithm showed good convergence properties. The objective function convergence history is exemplified for case GBJFR 1 in Fig. 3. In general, about 8–12 optimization steps were needed to converge the overall optimization process. For all the considered cases, the population size was equal to 200, the number of design variables was equal to 54, and the average number of generations run per GA optimization search was equal to 2000. It was verified that the increase in the population size does not lead to a higher accuracy of search.

The number of Navier–Stokes computations per optimization step was equal to 63 (54 for the database construction stage and 9 for the verification stage). The computations were performed on a computer cluster with IBM BladeCenter processors. In terms of wall-clock time consumption, one single-point optimization requires (on the available cluster) about 15–18 h.

It is worthwhile to note that, similar to the previously reported optimizations of simpler aerodynamic shapes performed with OPTIMAS (see [18–21,33]), all the results presented here are "first-shot" runs without the need for tuning any optimization/grid parameter.

The considered design point possesses a high freestream Mach number and a moderate transonic C_L value: $M = 0.80$ and $C_L = 0.40$. For the original configuration, this combination of flight conditions, as can be seen from the corresponding pressure distributions on the upper wing surface (Fig. 4) and at the fairing region (Fig. 5), leads to the development of a λ-like spanwise shock development. For convenience, the fairing part is visualized in Figs. 4 and 5, in which the positions of boundaries between the fairing and the inboard/outboard of fairing are indicated by solid lines. At these conditions, the drag value for the original configuration is equal to $C_D = 292.0$ aerodynamic counts.

The performed unconstrained (with respect to C_M and local thickness values) one-point wing optimization with the frozen fillet surface (labeled as case GBJ 2 in [21]) achieved 16.7 counts of drag reduction and decreased the total drag down to 275.3 counts. From the corresponding pressure distributions (Figs. 6 and 7), it can be concluded that the achieved drag reduction may be attributed to a significant decrease in the shock strength in the exposed-wing region.

At the same time, this optimization did not practically diminish the shock intensity at the wing–body–fairing region. This conclusion

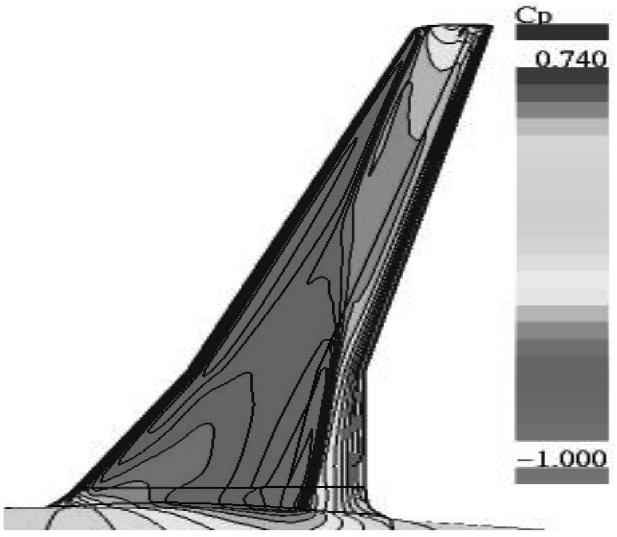

Fig. 4 Generic business jet pressure distribution on the wing upper surface at $M = 0.80$ and $C_L = 0.4$ for the original configuration.

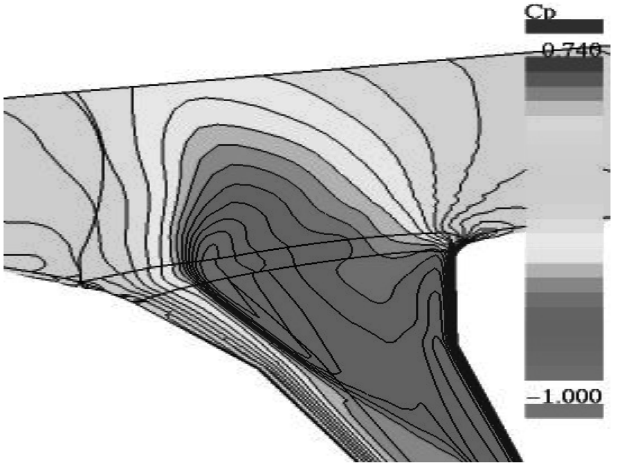

Fig. 5 Generic business jet pressure distribution at the wing–body–fairing region at $M = 0.80$ and$C_L = 0.4$ for the original configuration.

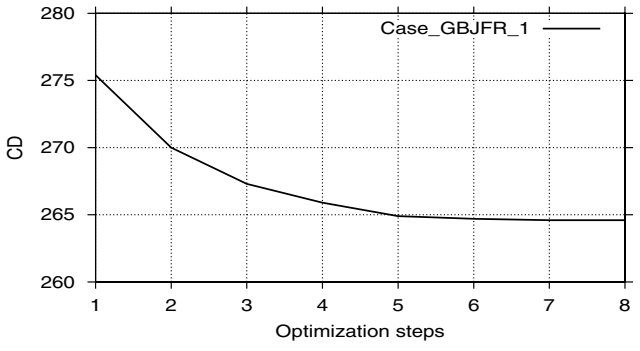

Fig. 3 Generic business jet convergence history of the optimization process for case GBJFR 1.

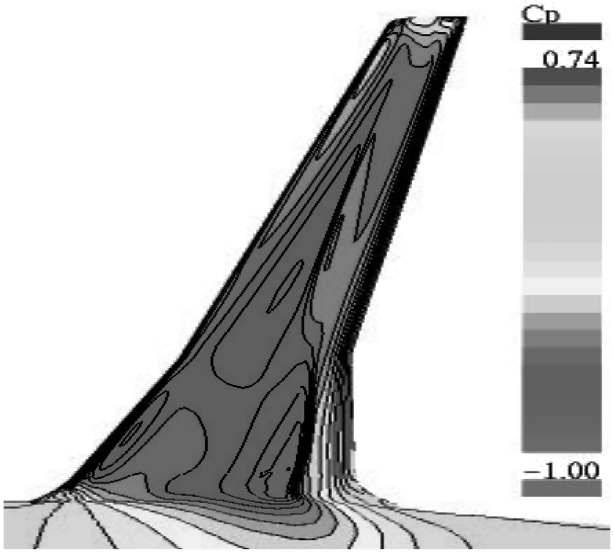

Fig. 6 Generic business jet pressure distribution on the wing upper surface at $M = 0.80$ and $C_L = 0.4$ for the optimized configuration case GBJ 2.

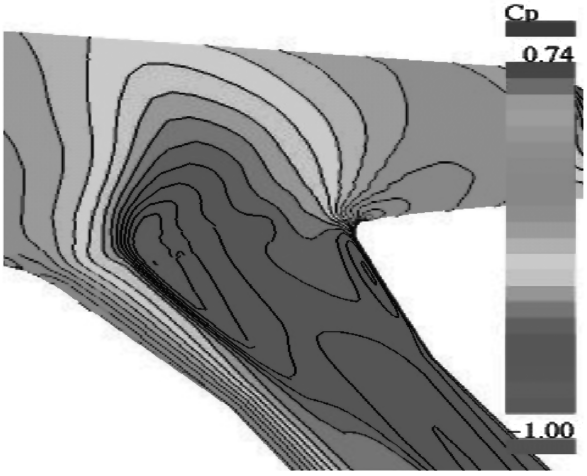

Fig. 7 Generic business jet pressure distribution at the wing–body–fairing region at $M = 0.80$ and $C_L = 0.4$ for the optimized configuration case GBJ 2.

may be drawn from the comparison between the corresponding chordwise pressure distributions at the spanwise coordinate $2y/b = 0.135$ located in the middle of the fairing region (see Fig. 8).

The optimization of the wing–body–fairing shape (case GBJFR 1) improved the pressure distribution in the fillet region. As can be seen from Figs. 9–11, this optimization essentially diminished the shock strength in the fairing-wing junction while preserving an acceptable flow pattern on the exposed wing. As a result, this improvement permits reducing the total drag of the optimized configuration by an additional 10.7 counts (compare with case GBJ 2) and achieving the level $C_D = 264.6$ counts.

The shape achieved by the fillet optimization (case GBJFR 1) is shown in Fig. 12, in which nondimensional sectional cuts of the optimal fairing are depicted. We see that optimal sectional shapes of the fillet tend to develop a convex–concave form on the upper surface, which is further enhanced in the outboard direction. Note that frequently, in aerodynamic practice, the upper surface of the wing root profile has a convex–concave form. Here, the optimizer discovered this trend automatically. Additionally, the trailing-edge cusp (nonexisting near the fuselage) becomes significant at the sections close to the exposed wing.

The second test case (case GBJFR 2), starting from case GBJFR 1 as an initial geometry, deals with the optimization of the exposed

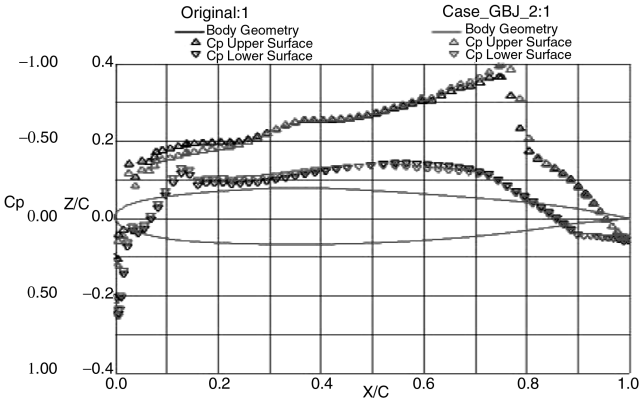

Fig. 8 Generic business jet chordwise pressure distribution at $M = 0.80$ and $C_L = 0.4$ at $2y/b = 0.135$ for original configuration vs case GBJ 2 .

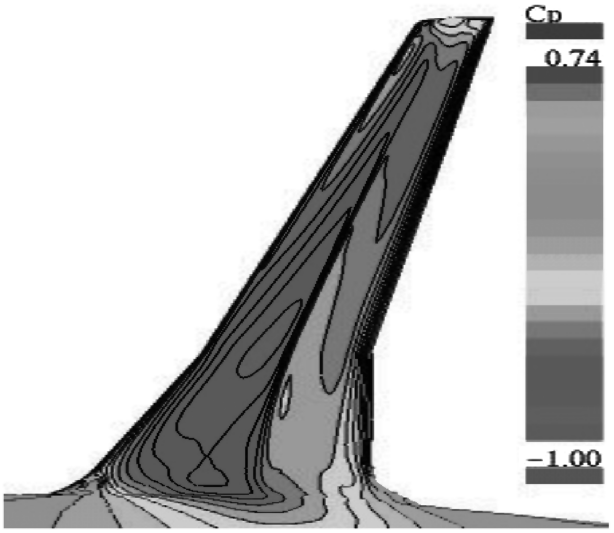

Fig. 9 Generic business jet pressure distribution on the wing upper surface at $M = 0.80$ and $C_L = 0.4$ for optimized configuration case GBJFR 1.

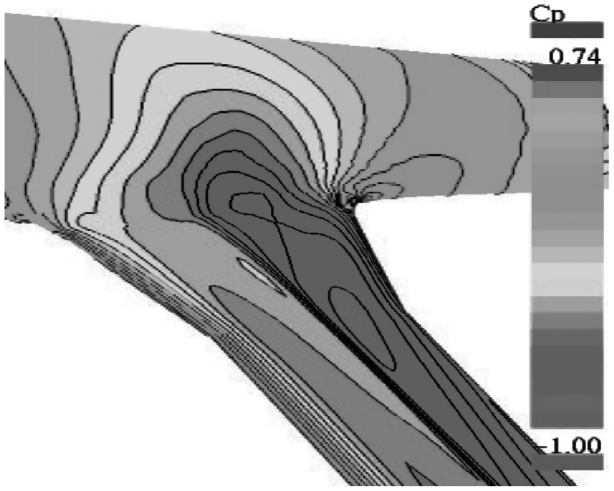

Fig. 10 Generic business jet pressure distribution at the wing–body–fairing region at $M = 0.80$ and $C_L = 0.4$ for optimized configuration case GBJFR 1.

wing, keeping the fairing shape frozen. Data illustrating the results achieved in the framework of this optimization are given in Figs. 13–16. We see that the strength of the shock in the flow over the optimized business jet (case GBJFR 2) has significantly decreased.

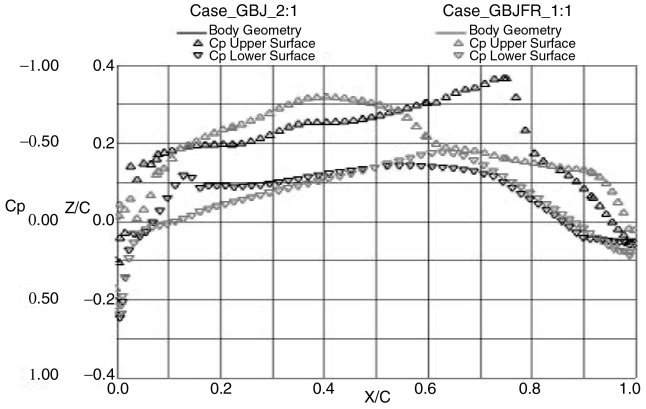

Fig. 11 Generic business jet chordwise pressure distribution at $M = 0.80$ and $C_L = 0.4$ at $2y/b = 0.135$ for optimized configuration case GBJFR 1 vs case GBJ 2.

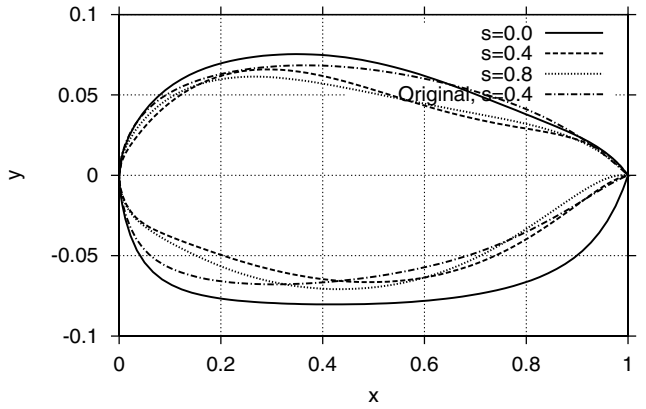

Fig. 12 Generic business jet shape of sectional cuts at the fairing region for optimized configuration case GBJFR 1.

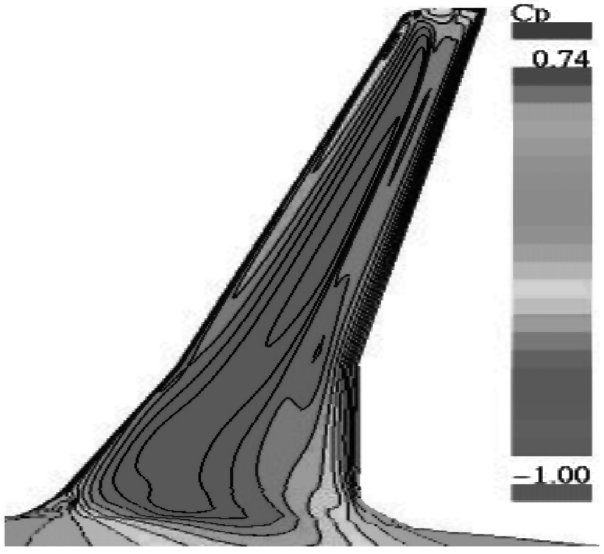

Fig. 13 Generic business jet pressure distribution on the wing upper surface at $M = 0.80$ and $C_L = 0.4$ for optimized configuration case GBJFR 2.

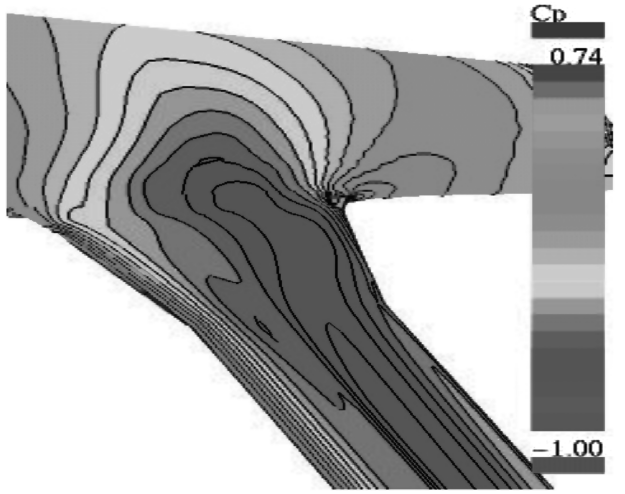

Fig. 14 Generic business jet pressure distribution at the wing–body–fairing region at $M = 0.80$ and $C_L = 0.4$ for optimized configuration case GBJFR 2.

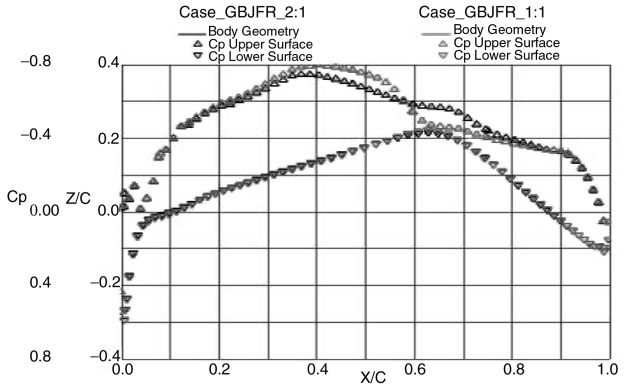

Fig. 15 Generic business jet chordwise pressure distribution at $M = 0.80$ and $C_L = 0.4$ at $2y/b = 0.135$ for optimized configuration case GBJFR 2 vs case GBJFR 2.

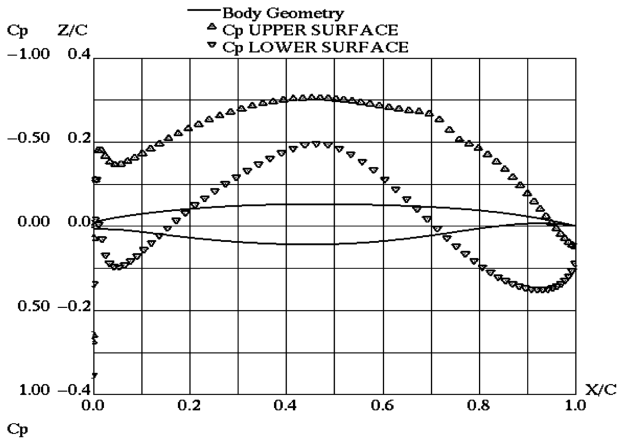

Fig. 16 Generic business jet chordwise pressure distribution at $M = 0.80$ and $C_L = 0.4$ at $2y/b = 0.48$ for optimized configuration case GBJFR 2.

The optimization case GBJFR 2 further improved the aerodynamic performance of the aircraft configuration: the total drag value is equal to 258.7 drag counts (5.9 counts less than that of the initial geometry case GBJFR 1).

From an aerodynamic point of view, it is interesting to estimate the contribution of each of the optimized surfaces (wing fairing and exposed wing) to a buildup of the gain due to optimization. The corresponding data can be found in Table 2, in which C_D values related to the exposed wing and the fairing region for different test cases are given. The following conclusions can be reached by analyzing Table 2. First, although it significantly reduced the wing drag, the exposed-wing optimization with the original frozen fillet (case GBJ 2) was less successful in terms of the total drag (the

Table 2 C_D value related to different parts of the aircraft geometry for different optimization cases (in aerodynamic counts)

	Original	GBJ 2	GBJFR 1	GBJFR 2	GBJFR 3	GBJFR 4
Wing	116.1	99.4	99.5	93.8	101.7	92.8
Fairing	49.2	49.2	38.5	38.3	40.0	39.0
Total	292.0	275.3	264.6	258.7	269.2	259.1

reduction was only about 50% from the ultimate reduction achieved by case GBJFR 2). The optimization of case GBJFR 1, in which only the fillet surface was subject to modification with the wing shape frozen, reduced about 11 counts of the fairing drag with almost no penalty on the wing drag. Finally, the optimization of case GBJFR 2, which corrected the wing shape in the presence of the new fillet, increased the drag reduction by an additional six counts. It is important to also note that in this case, the drag of the frozen parts of the aircraft did not increase.

Offdesign behavior of the optimized configurations may be studied through lift/drag polars. These are presented in Fig. 17, in which the corresponding curves at $M = 0.80$ are compared with the original polars. It can be concluded that the preceding local gains are preserved in a wide range of lift coefficient values from $C_L = 0.15$ to above 0.6. Additionally we should note that the drag reduction due to optimization increased for Mach numbers higher than the design value. Specifically, at $M = 0.82$ and $C_L = 0.40$, the drag reduction of case GBJFR 2, with respect to the original business jet configuration, is equal to 42 counts.

In terms of shape modification, the influence of the optimization parameters on the specific form of the crank and tip wing sections can be assessed from Figs. 18 and 19, in which the corresponding optimal nondimensional shapes of case GBJFR 2 vs case GBJFR 1 are depicted. Along with the unconstrained (with respect to C_M and local thickness) optimizations, the optimizations with beam constraints and with a constraint on the pitching moment were performed. In case GBJFR 3 and case GBJFR 4, the value of C_M^* and the relative wing thickness at the two fixed x/c locations were kept to the original level.

For case GBJFXR 3 (fairing optimization with frozen optimal wing), the initial geometry was the optimal shape of the one-point constrained drag minimization of the exposed wing, with fixed fuselage and fairing surfaces (labeled as case GBJ 5 in [21]). The total drag value for case GBJ 5 configuration was equal to 276.1 counts, and the fairing optimization reached the level of 269.2 drag counts (in total, about seven counts of drag reduction).

To clarify the influence of constraints on the results of the fairing optimization, let us compare test case GBJFR 3 (with constraints on local thickness and on C_M) vs case GBJFR 1 (no constraints). We see that in terms of drag reduction, the penalty due to the imposition of the constraints is about 4.6 counts. The more detailed analysis of the corresponding sectional chordwise pressure distributions (see Fig. 20 at $2y/b = 0.135$) demonstrates that this penalty may be attributed to a slightly weaker decrease in the shock strength

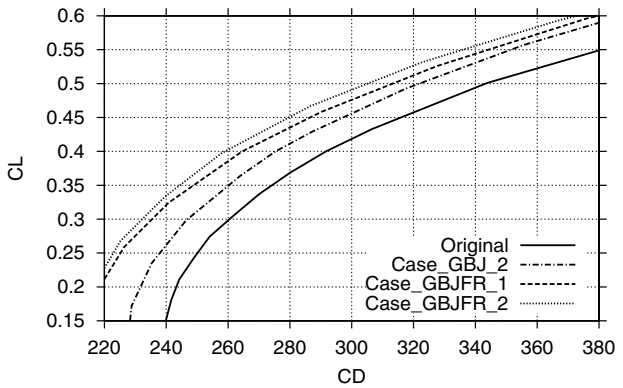

Fig. 17 Generic business jet drag polars at $M = 0.80$ for the original configuration vs optimized configuraitons.

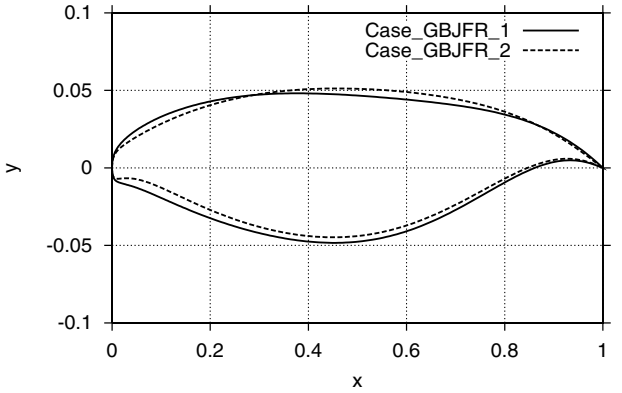

Fig. 18 Generic business jet shape of sectional wing cuts at $2y/b = 0.37$ for case GBJFR 1 vs case GBJFR 2.

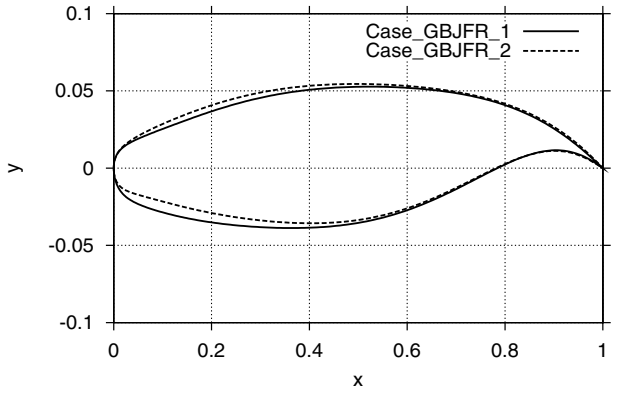

Fig. 19 Generic business jet shape of tip wing section for case GBJFR 1 vs case GBJFR 2.

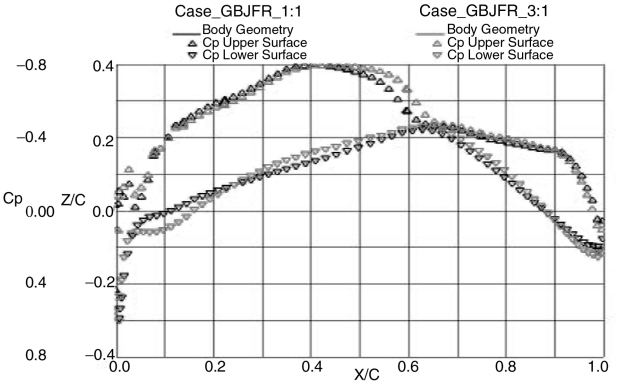

Fig. 20 Generic business jet chordwise pressure distribution at $M = 0.80$ and $C_L = 0.4$ at $2y/b = 0.135$ for optimized configuration case GBJFR 3 vs case GBJFR 1.

achieved by the constrained fairing optimization in comparison with the corresponding unconstrained optimization. Additionally, it is noted that the constrained fairing optimization is able to decrease the shock intensity not only at the design conditions, but also at a higher Mach number.

As for the optimal fairing shape, the comparison between fillet sectional cuts (Fig. 21 vs Fig. 22) shows that the corresponding shapes are close to each other, perhaps with a more pronounced droop effect in the neighborhood of the outboard fairing section for case GBJFR 3.

As mentioned in the Introduction, the current dominant practice is to use the Euler equations as the gas-dynamic model for aerodynamic shape optimizations. In this respect, to check the influence of the gas-dynamic model on the results of the optimization, we performed an

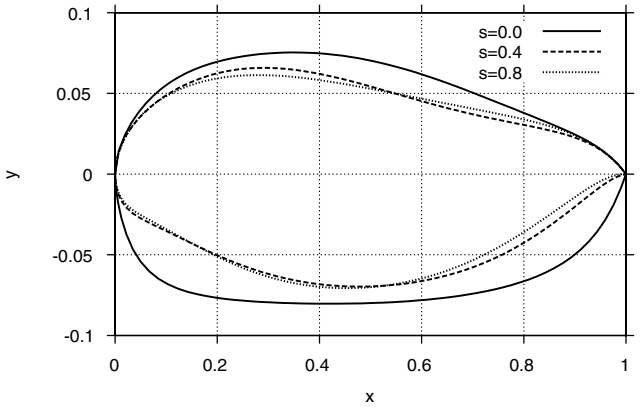

Fig. 21 Generic business jet shape of sectional cuts in the fairing region for optimized configuration case GBJFR 3.

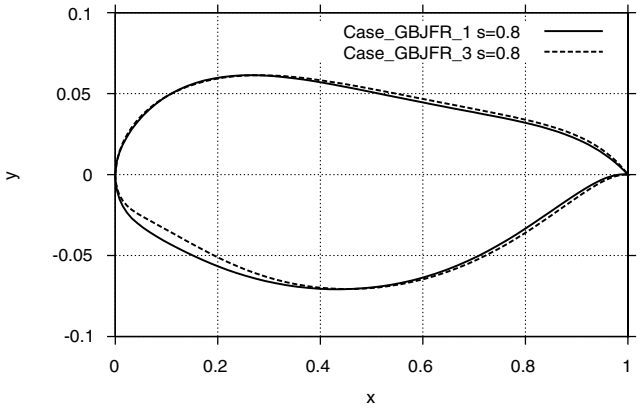

Fig. 22 Generic business jet shape of sectional cuts in the fairing region for case GBJFR 1 vs case GBJFR 3.

optimization of the wing–body fairing based on the numerical solution of the Euler equations (contrary to case GBJFR 3, in which the CFD driver of the optimization was Navier–Stokes computations). For consistency of comparison, the Euler-based optimal geometry obtained was verified via numerical solution of the Navier–Stokes equations.

The results were as follows. The total drag value achieved by this Euler-driven optimization of the wing–fairing region was equal to 312.9 counts, compared with 269.2 counts for case GBJFR 3. Moreover, the resulting drag coefficient is higher not only with respect to C_D of the initial geometry (case GBJ 5), but is also about 20 counts higher than the total drag of the original business jet configuration.

The analysis of the corresponding pressure distributions (see Figs. 23 and 24) demonstrates that instead of decreasing the shock intensity, the Euler equations drive the optimization in the wrong direction, which leads to an essentially higher shock level for the corresponding optimal configuration. It is the authors' opinion that the reason lies in the inability of inviscid (Euler) flow simulation to accurately treat shock/boundary-layer interaction, which is of high significance in the region of the body–fairing–wing junction. As a consequence, the Euler-driven optimization excessively enhanced the convex–concave tendency on the upper surface of the optimized fillet, which resulted in a shape optimal from the point of view of the inviscid gas-dynamic model, but which fully failed through the verification by an accurate high-fidelity viscous numerical simulation. This means that when viscous effects are significant, an optimization should be driven by an adequate viscous gas-dynamic model (in this case, the full Navier–Stokes equations).

Let us now consider the results achieved in the last test case GBJFR 4. Starting from the case GBJFR 3 aircraft shape as an initial geometry, this constrained optimization deals with the

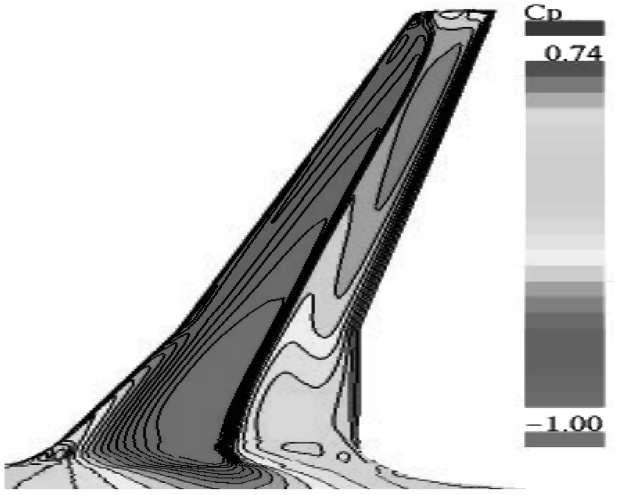

Fig. 23 Generic business jet pressure distribution on the wing upper surface for $M = 0.80$ and $C_L = 0.4$ for the optimized configuration driven by Euler equations.

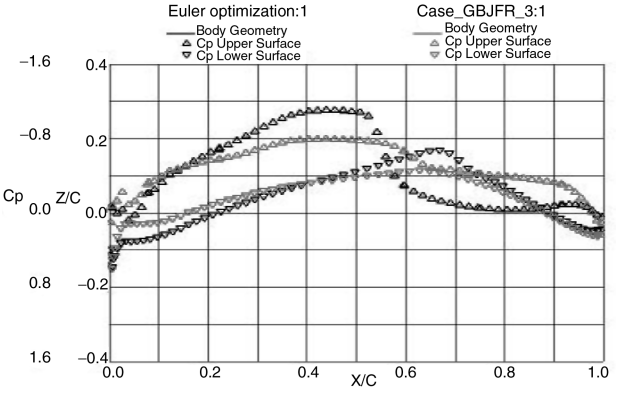

Fig. 24 Generic business jet chordwise pressure distribution at $M = 0.80$ and $C_L = 0.4$ at $2y/b = 0.135$ for Euler-driven fairing optimization vs case GBJFR 3.

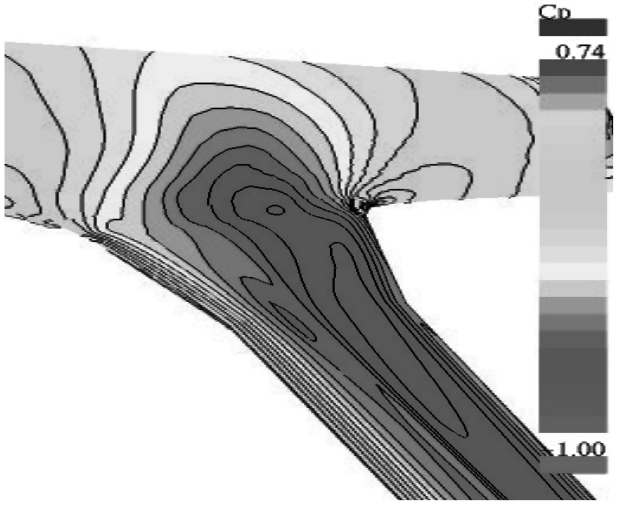

Fig. 25 Generic business jet pressure distribution at the wing–body–fairing region at $M = 0.80$ and $C_L = 0.4$ for optimized configuration case GBJFR 4.

modification of the exposed wing, keeping the wing–body fillet shape frozen. Graphical data for this test case are presented in Figs. 25–28. The pressure distributions on the upper surface of the exposed wing and on the fillet for $M = 0.80$ are presented in Figs. 25

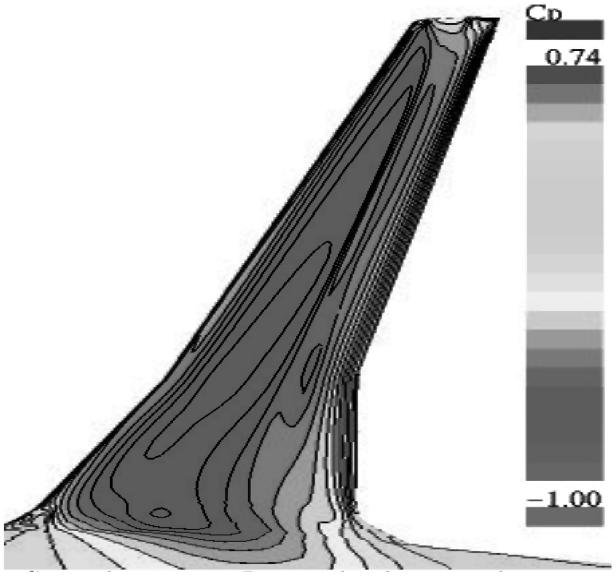

Fig. 26 Generic business jet pressure distribution on the wing upper surface at $M = 0.80$ and $C_L = 0.4$ for optimized configuration case GBJFR 4.

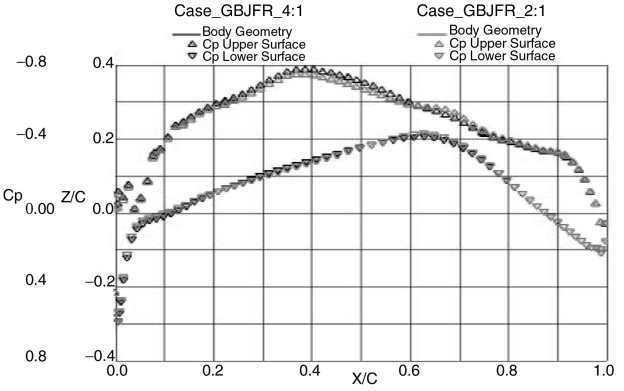

Fig. 27 Generic business jet chordwise pressure distribution at $M = 0.80$ and $C_L = 0.4$ at $2y/b = 0.135$ for optimized configuration case GBJFR 4 vs case GBJFR 2.

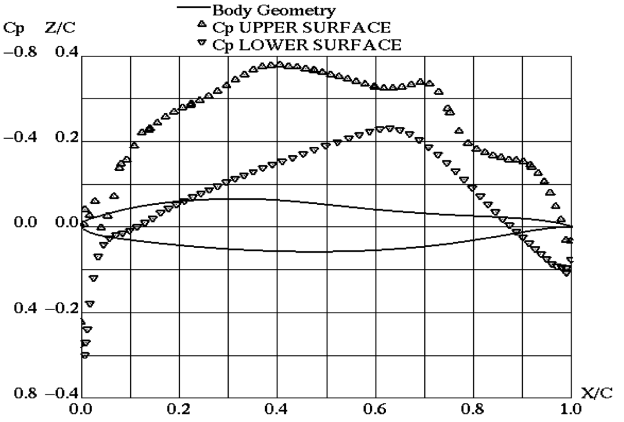

Fig. 28 Generic business jet chordwise pressure distribution at $M = 0.82$ and $C_L = 0.4$ at $2y/b = 0.135$ for optimized configuration case GBJFR 4.

and 26, and chordwise C_P sectional distributions are shown in Figs. 27 and 28.

The corresponding drag reduction was equal to 10.1 counts. It is important to note that the achieved drag level ($C_D = 259.1$ counts and $C_M = -0.136$) is only a little bit higher than with case GBJFR 2 ($C_D = 258.7$ counts and $C_M = -0.149$). This means that in the framework of the successive optimizations of the exposed wing and of the fillet region, the penalty due to the imposition of the pitching moment constraint and beam constraints is negligibly small (about 0.4 counts). Moreover, at a higher Mach number ($M = 0.82$), the drag reduction for case GBJFR 4 compared with the original aircraft configuration was equal to 42.7 counts (from the original 321.5 counts down to 278.8 counts), and the total drag value for case GBJFR 2 was equal to 280.8 aerodynamic counts.

The influence of the constraints imposition on the optimized shapes vs the unconstrained optimization may be assessed from the comparisons of Fig. 18 vs Fig. 19 and Fig. 29 vs Fig. 30. It can be observed that the requirements coming from the constraints imposition resulted in a significant reshape of the crank and tip sections, especially on the lower surface at the leading-edge region. From both the theoretical and practical points of view, it is interesting to determine whether the optimal shapes are unique. The preceding comparison of optimal shapes provides a clarifying example on the subject. We see that very close values of total drag may correspond to significantly different geometries.

Finally, let us present data that illustrate the offdesign behavior of the optimal geometry of case GBJFR 4: lift/drag polars at $M = 0.80$ and 0.82 (Figs. 31 and 32) and Mach drag rise curves at the design $C_L = 0.4$ (Fig. 33). As a whole, the analysis of these figures shows that the considered optimization is not restricted to a single design point and that the gain due to optimization is observed in a wide region of lift values and freestream Mach numbers. For example, the optimization succeeded in shifting the Mach drag divergence point to at least the main Mach design value. Specifically, based on the definition of the Mach drag divergence point as the Mach value at which $\partial C_D/\partial M = 0.1$, the corresponding M_{DD} value for the original configuration is equal to 0.795, and for case GBJFR 2 and

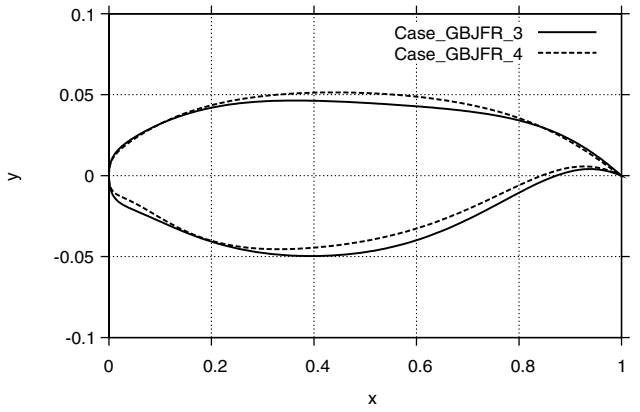

Fig. 29 Generic business jet shape of sectional wing cuts at $2y/b = 0.37$ for case GBJFR 3 vs case GBJFR 4.

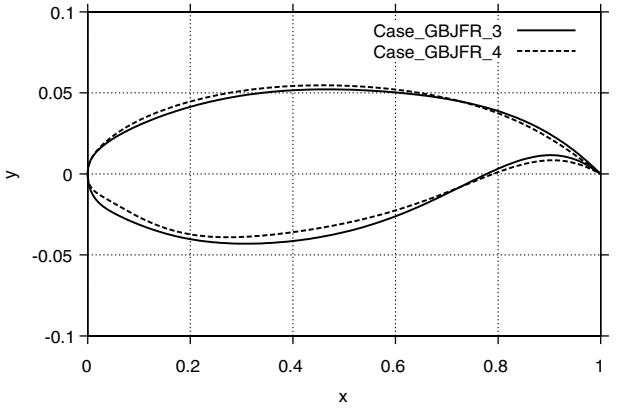

Fig. 30 Generic business jet shape of tip wing section for case GBJFR 3 vs case GBJFR 4.

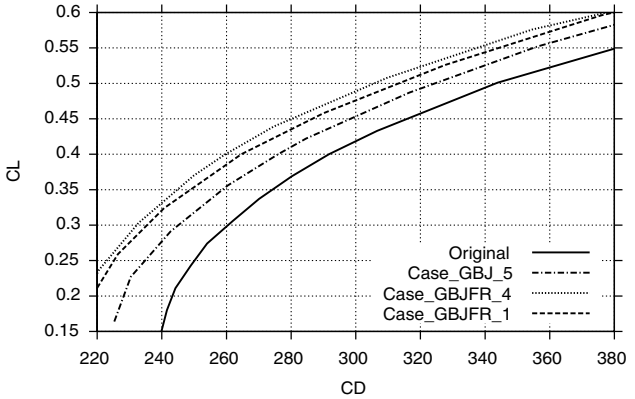

Fig. 31 Generic business jet drag polars at $M = 0.80$ for the original configuration vs optimized configurations.

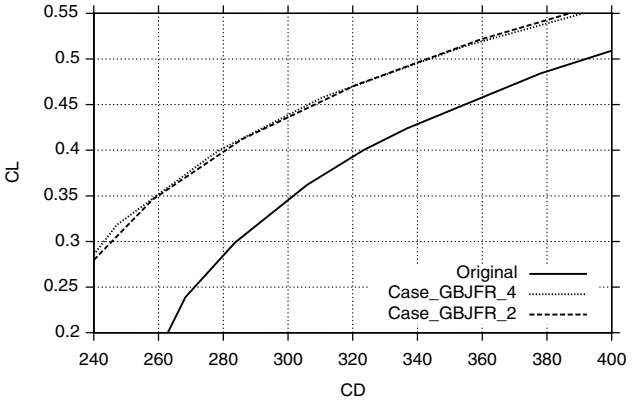

Fig. 32 Generic business jet drag polars at $M = 0.82$ for the original configuration vs optimized configurations.

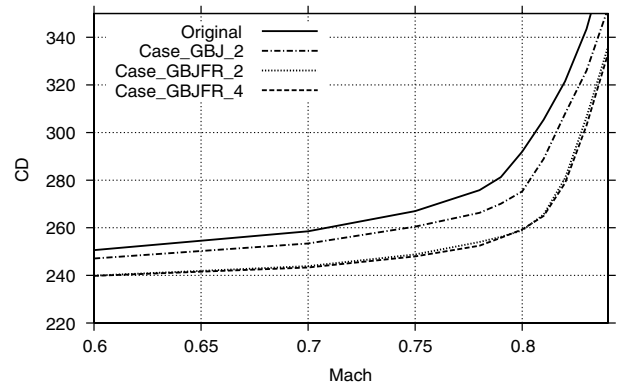

Fig. 33 Generic business jet Mach drag divergence for the original configuration vs optimized configurations.

case GBJFR 4 $M_{DD} = 0.815$. Additionally, the subsonic drag level of the optimized configuration is also decreased (apparently due to reduction in the value of form drag).

V. Conclusions

A new approach for optimization of essentially 3-D aerodynamic shapes for minimum drag is proposed. The method handles nonlinear surfaces typical of complex aircraft junctions such as wing–body fairings. The optimization framework OPTIMAS, previously proposed by the authors for the solution of drag-minimization problems, is extended to a significantly higher level of geometrical complexity. The method is applied to optimization of the wing–body fairing for generic business jet configuration at realistic transonic cruise flight conditions. The results demonstrate that the proposed approach achieves significant drag reduction in on- and offdesign conditions.

References

[1] Lighthill, M. J., *A New Method of Two-Dimensional Aerodynamic Design*, Aeronautical Research Council, Reports and Memoranda No. 1111, London, 1945.

[2] Alexandrov, N. M., Lewis, R. M., Gumbert, C. R., Green, L. L., and Newman, P. A., "Approximation and Model Management in Aerodynamic Optimization with Variable Fidelity Models," *Journal of Aircraft*, Vol. 38, No. 6, 2001, pp. 1093–1101.

[3] Bauer, F., Garabedian, P., Korn, D., and Jameson, A., *Supercritical Wing Sections 2*, Springer–Verlag, New York, 1975.

[4] Giles, M. B., and Drela, M., "Two-Dimensional Transonic Aerodynamic Design Method," *AIAA Journal*, Vol. 25, No. 9, 1987, pp. 1199–1206.

[5] Drela, M., "A User's Guide to MSES V2.6," MIT Computational Aerospace Sciences Lab., Cambridge, MA, 1994.

[6] Jameson, A., "Optimum Aerodynamic Design Using Control Theory," *Computational Fluid Dynamics Review*, Wiley, New York, 1995, pp. 495–528.

[7] Mohammadi, B., and Pironneau, O., *Applied Shape Optimization for Fluids*, Oxford Univ. Press, Oxford, 2001.

[8] Jameson, A., Martinelli, L., and Pierce, N., "Optimum Aerodynamic Design Using Navier–Stokes Equations," *Theoretical and Computational Fluid Dynamics*, Vol. 10, No. 1, 1998, pp. 213–237. doi:10.1007/s001620050060

[9] Nielsen, E., and Anderson, W., "Aerodynamic Design Optimization on Unstructured Meshes Using the Navier–Stokes Equations," *AIAA Journal*, Vol. 37, No. 11, 1999, pp. 1411–1419.

[10] Le Moigne, A., and Qin, N., "Variable Fidelity Aerodynamic Optimization for Turbulent Flows Using a Discrete Adjoint Formulation," *AIAA Journal*, Vol. 42, No. 7, 2004, pp. 1281–1292. doi:10.2514/1.2109

[11] Le Moigne, A., and Qin, N., "Airfoil Profile and Sweep Optimization for a Blended Wing-Body Aircraft Using a Discrete Adjoint Method," *The Aeronautical Journal*, Vol. 110, Sept. 2006, pp. 589–604.

[12] Jameson, A., Martinelli, L., and Vassberg, J., "Using Computational Fluid Dynamics for Aerodynamics—A Critical Assessment," International Council of the Aeronautical Sciences Paper 2002-1.10.1, 2002.

[13] Jameson, A., "The Role of CFD in Preliminary Aerospace Design," 4th ASME/JSME Joint Fluids Engineering Conference, Honolulu, HI, American Society of Mechanical Engineers, Fluids Engineering Div., Paper 2003-45812, July 2003.

[14] Yamazaki, W., Matsushima, K., and Nakahashi, K., "Drag Reduction of a Near-Sonic Airplane Using Computational Fluid Dynamics," *AIAA Journal*, Vol. 43, No. 9, 2005, pp. 1870–1877. doi:10.2514/1.15059

[15] Pironneau, O., *Optimal Shape Design for Elliptic Systems*, Springer–Verlag, New York, 1984.

[16] Obayashi, S., Yamaguchi, Y., and Nakamura, T., "Multiobjective Genetic Algorithm for Multidisciplinary Design of Transonic Wing Planform," *Journal of Aircraft*, Vol. 34, No. 5, 1997, pp. 690–693.

[17] Hajela, P., "Nongradient Methods in Multidisciplinary Design Optimization—Status and Potential," *Journal of Aircraft*, Vol. 36, No. 1, 1999, pp. 255–265.

[18] Epstein, B., and Peigin, S., "Robust Hybrid Approach to Multiobjective Constrained Optimization in Aerodynamics," *AIAA Journal*, Vol. 42, No. 8, 2004, pp. 1572–1581. doi:10.2514/1.992

[19] Epstein, B., and Peigin, S., "Constrained Aerodynamic Optimization of Three-Dimensional Wings Driven by Navier–Stokes Computations," *AIAA Journal*, Vol. 43, No. 9, 2005, pp. 1946–1957. doi:10.2514/1.10308

[20] Peigin, S., and Epstein, B., "Computational Fluid Dynamics Driven Optimization of Blended Wing–Body Aircraft," *AIAA Journal*, Vol. 44, No. 11, 2006, pp. 2736–2745. doi:10.2514/1.19757

[21] Epstein, B., and Peigin, S., "Efficient Approach for Multipoint Aerodynamic Wing Design of Business Jet Aircraft," *AIAA Journal*, Vol. 45, No. 11, 2007, pp. 2612–2621.

[22] Baldwin, B. S., and Lomax, H., "Thin Layer Approximation and Algebraic Model for Separated Turbulent Flows," AIAA Paper 1978-0257, 1978.

[23] Epstein, B., Rubin, T., and Seror, S., "Accurate Multiblock Navier–Stokes Solver for Complex Aerodynamic Configurations," *AIAA Journal*, Vol. 41, No. 4, 2003, pp. 582–594.

[24] Shu, C.-W., and Osher, S., "Efficient Implementation of Essentially Nonoscillatory Shock-Capturing Schemes," *Journal of Computational Physics*, Vol. 83, No. 1, 1989, pp. 32–78. doi:10.1016/0021-9991(89)90222-2

[25] Annicchiarico, W., Periaux, J., Cerrolaza, M., and Winter, G., *Evolutionary Algorithms and Intelligent Tools in Engineering Optimization*, International Center for Numerical Methods in Engineering, Barcelona, 2004.

[26] Michalewicz, Z., *Genetic Algorithms + Data Structures = Evolution Programs*, Springer–Verlag, New York, 1996.

[27] Sefrioui, M., Periaux, J., and Ganascia, J. G., "Fast Convergence Thanks to Diversity," *Proceedings of the 5th Annual Conference on Evolutionary Programming*, MIT Press, Cambridge, MA, 1996, pp. 313–321.

[28] Peigin, S., and Epstein, B., "Robust Handling of Nonlinear Constraints for GA Optimization of Aerodynamic Shapes," *International Journal for Numerical Methods in Fluids*, Vol. 45, No. 12, 2004, pp. 1339–1362. doi:10.1002/fld.747

[29] Vicini, A., and Quagliarella, D., "Airfoil and Wing Design Through Hybrid Optimization Strategies," *AIAA Journal*, Vol. 37, No. 5, 1999, pp. 634–641.

[30] Dowell, E. H., "Eigen-Mode Analysis in Unsteady Aerodynamics: Reduced-Order models," *36th AIAA Structures, Structural Dynamics, and Materials Conference*, AIAA, Washington, D.C., 1995, pp. 2545–2557.

[31] Raveh, D. E., "Reduced-Order Models for Nonlinear Unsteady Aerodynamics," *AIAA Journal*, Vol. 39, No. 8, 2001, pp. 1417–1429.

[32] Peigin, S., and Epstein, B., "Embedded Parallelization Approach for Optimization in Aerodynamic Design," *Journal of Supercomputing*, Vol. 29, No. 3, 2004, pp. 243–263. doi:10.1023/B:SUPE.0000032780.68664.1b

[33] Peigin, S., and Epstein, B., "Robust Drag Minimization of Aerodynamic Wings in Engineering Environment," *Journal of Aircraft*, Vol. 43, No. 4, 2006, pp. 1195–1204. doi:10.2514/1.18634

A. Messac
Associate Editor